J Mater Sci (2007) 42:4785–4791
DOI 10.1007/s10853-006-0763-7

Synthesis by the solution combustion process and magnetic properties of iron oxide (Fe_3O_4 and α-Fe_2O_3) particles

Juliano Toniolo · Antonio S. Takimi · Mônica J. Andrade · Renato Bonadiman · Carlos P. Bergmann

Received: 13 January 2006 / Accepted: 4 August 2006 / Published online: 19 March 2007

Abstract This article describes the solution combustion synthesis technique as applicable to iron oxide powder production using urea as fuel and ferric nitrate as an oxidizer. It focuses on the thermodynamic modeling of the combustion reaction under different fuel-to-oxidant ratios. X-ray diffraction showed magnetite (Fe_3O_4) and hematite (α-Fe_2O_3) phase formations for the as-synthesized powders. The smallest crystallite size was obtained by stoichiometric chemical reaction. The magnetic properties of the samples are also carefully discussed as superparamagnetic behavior.

Introduction

The latest developments in functionalized magnetic nanosized particles show considerable promise for both enhanced and novel applications such as catalyst [1], pigment [2], sintering agent [3], photonic [4], drug [5], and biomedical [6] products.

Materials of interest to magnetically guidable systems are iron oxides such as γ-Fe_2O_3, Fe_3O_4 and $MO{\cdot}Fe_2O_3$ (where M is Mn, Co, Ni, or Cu) because they display ferrimagnetism. These iron oxides inherently display a lower magnetic response than ferromagnetic materials, such as the transition metals. However, the iron oxides are also less sensitive to oxidation and therefore maintain stable magnetic responses [7].

By and large, magnetite (Fe_3O_4) particles have been prepared by the co-precipitation of Fe^{2+} and Fe^{3+} chlorides in bulk aqueous solutions and surfactant systems [8]. Hematite (α-Fe_2O_3) particles are also obtained by precipitation under hydrolysis reaction [9]. Another method for forming magnetite particles by precipitation utilizes force mixing in aqueous solution without any surfactant [10].

An alternative method for the preparation of magnetic particles which offers outstanding characteristics is the solution combustion synthesis (SCS). This technique was introduced for oxide materials preparation two decades ago [11–14], but otherwise there have been not many studies into iron oxide particles [15–18].

As can be seen by examining the cited articles Patil and Sureh [15] were the first scientists to publish the instant synthesis of maghemite (γ-Fe_2O_3) by combustion process. After, the as-synthesized maghemite (γ-Fe_2O_3) was also studied by the Venkataraman et al. [16] via the combustion route. The authors illustrated by different techniques, including magnetism evaluation, the characterization of maghemite under different fuel-to-oxidant ratios.

Varma et al. [17, 18] have been reported two studies on aqueous combustion solution of Fe_3O_4, α- and γ-Fe_2O_3, for the first time in literature, using a variety of fuels hydrazine, urea, glycine and citric acid. However, they did not present results about the magnetization properties for α-Fe_2O_3 hematite powders.

On the other hand, the novelty of our work demonstrates that iron oxides powders (magnetite and hematite) were obtained by the urea-nitrate combustion process and their magnetic behavior were specially evaluated. The superparamagnetism of Fe_3O_4 and α-Fe_2O_3 powders obtained by solution combustion synthesis was not reported before and

J. Toniolo (✉) · A. S. Takimi · M. J. Andrade · R. Bonadiman · C. P. Bergmann
Department of Materials Engineering, Federal University of Rio Grande do Sul, 99 Osvaldo Aranha Av. 705, 90035190 Porto Alegre, RS, Brazil
e-mail: juliano.toniolo@br.bosch.com

this article differs from studies already published in the literature.

SCS is able to produce fine and homogeneous particles by atomization of the liquid before reaction and the explosive nature of the reaction itself. The reaction is an explosive process and extra precaution does need to be taken. The pyrolized powder that is left may be the single phase end product, but usually will be a combination of metal oxides as the ultimate result of the process. Homogeneity is achieved primarily because the system in solution is mixed on an atomic scale, and diffusion is therefore limited to the size of the liquid droplet before drying or combustion.

The success of the process is due to an intimate blending among the constituents using a suitable fuel or complexing agent (e.g., citric acid, urea, glycine, etc.) in an aqueous medium and an exothermic redox reaction between the fuel and an oxidizer (i.e., nitrates) [19].

Actually, hydrated nitrates were selected as the metals precursors: not only are they fundamental for the method, the NO_3^- groups being the oxidizing agents, but also their high solubility in water allows a proper homogenization.

Urea is a convenient fuel given that it promotes low crystallite sizes and acts as a complexing agent for the ferrous ion since it contains two amino groups at the end of the expected structure. As shown by Deshpande et al. [17] based on studies of iron nitrate with other fuels, the activity of a NH_2 type ligand appears to be the highest, where only the amino group triggers a vigorous combustion reaction.

For that reason, in the present work, we report the synthesis of iron oxide powders (Fe_3O_4 and α-Fe_2O_3) by different fuel-to-oxidant molar ratios using urea as a fuel and ferric nitrate as oxidizer. The effect of the fuel in controlling particle size and microstructure of the product for combustion under different fuel-to-oxidant ratios is investigated by a few scientists [20, 21].

The initial composition of the solution containing ferric nitrate and urea was derived from the total oxidizing and reducing valences of the oxidizer and fuel using the concepts of propellant chemistry [22]. Carbon, hydrogen and ferrous were considered as reducing species with the corresponding valences of +4, +1 and +3, respectively. Oxygen was considered as an oxidizing element with the valence of –2, nitrogen was considered to be 0. The total calculated valences of metal nitrates by arithmetic summation of oxidizing and reducing valences was –15. The calculated valence of urea was +6.

The stoichiometric composition of the redox mixture demanded that 4(–15) + n(+6) = 0, or n = 10 moles. Thus, the reactants were combined in the molar proportion of 4:10 or 1:2.5.

The powders obtained through SCS have been evaluated by scanning electron microscopy, X-ray diffraction and vibrating sample magnetometer analyses. Enthalpies were calculated theoretically for all reactions.

Experimental procedure

Ferric nitrate $Fe(NO_3)_3 \cdot 9H_2O$ (Synth Química, Brazil) and urea (Synth Química, Brazil) with 99% and 99.5% purities respectively (vendor specification) were employed as the starting materials.

The components are carefully dissolved in water, and the solution was subjected to the heating with the Bunsen-type burner continuously. Afterwards the urea-nitrate solution became transparent viscous gel which auto-ignited, giving a voluminous foam as product of the combustion. The flowchart for the process is shown in Fig. 1.

Each experiment was carried out in a stainless steel container. In order to avoid gas escape an exhaust hood was employed. The temperatures of the combustion were measured using an adjustable type K thermocouple.

The as-synthesized powders, without any kind of additional treatment, were characterized by X-ray diffraction (XRD), scanning electron microscopy (SEM), and vibrating sample magnetometer (VSM) measurements.

X-ray diffraction was executed on the combustion-synthesized powders for phase characterization, at a rate of 1°/min, using Cu-K_α radiation on a Philips X-ray diffractometer, (model X'Pert MPD).

The relative phase abundances of different phases have been estimated by Rietveld's powder structure refinement analysis of XRD data. Crystallite sizes were obtained by

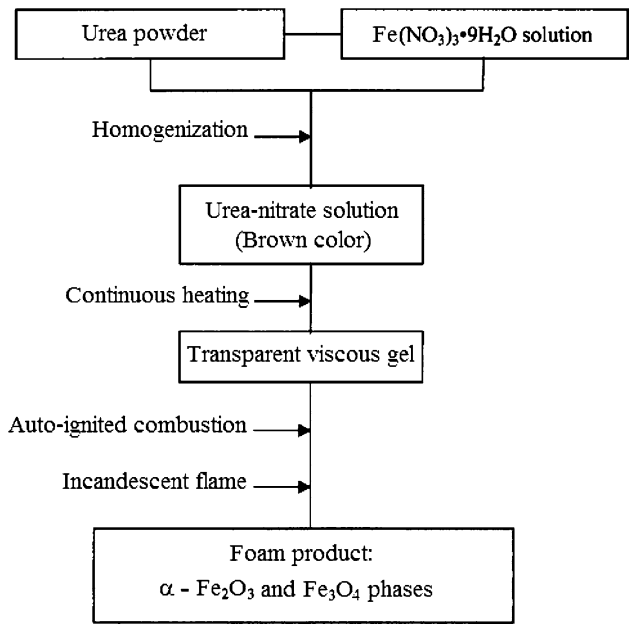

Fig. 1 Flowchart for the preparation of iron oxide powders

X-ray diffraction line broadening through single-line plot, assuming Pearson VII profile for size contribution. These data were analyzed using the WinFit software (version 1.2.1).

Scanning electron micrographs were recorded with a Jeol (model JSM-5800) instrument after coating the samples with gold.

Vibratory sample magnetometer, shown schematically in Fig. 2, was the instrument utilized for characterizing the magnetic behavior of the samples. It employs an electromagnet which provides the magnetizing field (DC), a vibrator mechanism to vibrate the sample in the magnetic field, and detection coils which generate the signal voltage due to the changing flux emanating from the vibrating sample. The output measurement displays the magnetic moment M as a function of the field H. This applied magnetic field was varied from –15,000 Oe to 15,000 Oe.

In order to prepare the samples under different fuel-to-oxidant ratios, we set the samples into thin capillary glass columns (Ø 6 mm) that were properly coupled with the vibrating equipment.

Results and discussion

Thermodynamic modeling

The chemical precursors are geared to the needs of SCS. This technique takes into account that urea and ferric nitrate decompose by assuming their thermodynamic modeling as well. The decomposition reaction of 1 mol of urea leads to the evolution of different gases, while ferric nitrate also includes the formation of iron oxides (such as Eqs. 1 and 2).

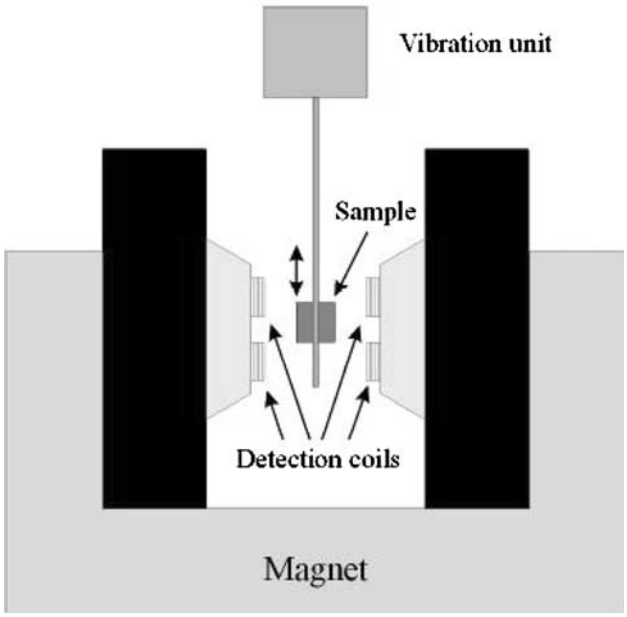

Fig. 2 Schematic diagram of the VSM

$$CO(NH_2)_2 + O_2 \rightarrow CO_2 + 2.0\,H_2O + N_2 \quad (1)$$

$$4.0Fe(NO_3)_3 \cdot 9H_2O \rightarrow 3.0Fe_2O_3 + 2.0Fe_3O_4 + 135.5O_2 + 6.0N_2 + 36H_2O \quad (2)$$

From a thermodynamic point of view, the chemical reaction of ferric nitrate along with urea can be done under various conditions, leading to the evolution of different products, as follows: bi-phase constitution (Fe_3O_4 and α-Fe_2O_3), or only a single-phase (α-Fe_2O_3 or Fe_3O_4). The overall combustion reactions are represented, correspondingly, in this way:

Stoichiometry (S)

$$4.0Fe(NO_3)_3 \cdot 9H_2O + 10.0CO(NH_2)_2 \rightarrow 3.0Fe_2O_3 + 2.0Fe_3O_4 + 125.5O_2 + 16.0N_2 + 56H_2O \quad (3)$$

Fuel-lean (–50%, L1)

$$4.0Fe(NO_3)_3 \cdot 9H_2O + 5.0CO(NH_2)_2 \rightarrow 3.0Fe_2O_3 + 2.0Fe_3O_4 + 130.5O_2 + 11.0N_2 + 46.0H_2O + 50CO_2 \quad (4)$$

Fuel-rich (+100%, R1)

$$4.0Fe(NO_3)_3 \cdot 9\,H_2O + 20.0CO(NH_2)_2 \rightarrow 3.0Fe_2O_3 + 2.0Fe_3O_4 + 115.5O_2 + 26.0N_2 + 76.0H_2O + 20.0CO_2 \quad (5)$$

Fuel-rich (+200%, R2)

$$4.0Fe(NO_3)_3 \cdot 9H_2O + 27.0CO(NH_2)_2 \rightarrow 3.0Fe_2O_3 + 2.0Fe_3O_4 + 108.5O_2 + 33.0N_2 + 90.0H_2O + 27.0CO_2 \quad (6)$$

Fuel-rich (+300%, R3)

$$4.0Fe(NO_3)_3 \cdot 9H_2O + 40.0CO(NH_2)_2 \rightarrow 3.0Fe_2O_3 + 2.0Fe_3O_4 + 95.5O_2 + 46.0N_2 + 116.0H_2O + 40.0CO_2 \quad (7)$$

Fuel-rich (+500%, R4)

$$4.0Fe(NO_3)_3 \cdot 9H_2O + 60.0CO(NH_2)_2 \rightarrow 3.0Fe_2O_3 + 2.0Fe_3O_4 + 75.5O_2 + 66.0N_2 + 156.0H_2O + 60.0CO_2 \quad (8)$$

The presence of N_2 and O_2 from air has not been taken into account in the reactions described. Using the thermodynamic data for various reactants and products listed in Table 1, the enthalpy of combustion as a function of urea-to-nitrate molar ratio can be calculated as showed in Fig. 3.

Phase formation and morphology

Figure 4 exhibits the X-ray diffraction patterns of iron oxide powders synthesized under different fuel-to-oxidant ratios.

The fuel-lean ratio (L1) was analyzed and it revealed a slight crystallization of hematite phase, remaining the amorphous formation.

The phase formation of magnetite occurs only with stoichiometric (S) and fuel-rich ratios (R1, R2, R3 and R4).

As fuel is added, the magnetite phase increases until it reaches a maximum level. The phase then starts to decrease. In reality, this behavior was followed reliably as seen by R4 in Fig. 4. Based on this behavior we will not expect that the maximum fuel-rich ratio could lead to the highest formation in situ of the magnetite crystalline phase. Under the fuel-rich condition, many fuel-to-oxidant ratios have been tested and led to a reasonable quantity of both iron oxides: hematite and magnetite.

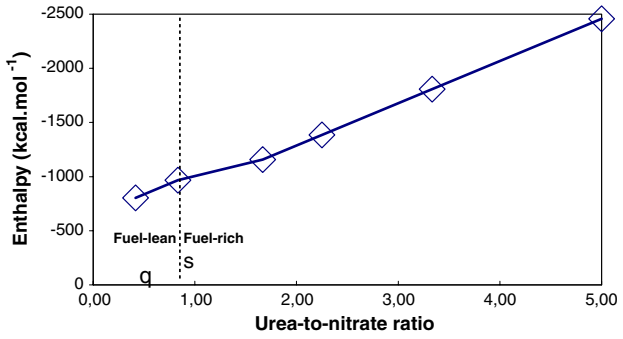

Fig. 3 Variation of enthalpy as a function of urea-to-nitrate molar ratio

Table 1 Relevant thermodynamics data [23, 24]

Compound[a]	ΔH_f (kcal mol^{-1}) at 25 °C	Cp (Cal mol^{-1} K^{-1})
$Fe(NO_3)_3 \cdot 9H_2O$ (c)	–160.37	–
$CO(NH_2)_2$ (c)	–79.71	–
Fe_2O_3 (c)	–198.5	31.70 + 0.00176 T[b]
Fe_3O_4 (c)	–266.9	21.88 + 0.0482 T[b]
CO_2 (g)	–94.051	10.34 + 0.00274 T[b]
N_2 (g)	0	6.50 + 0.0010 T[b]
O_2 (g)	0	5.92 + 0.00367 T[b,c]
H_2O (g)	–57.796	7.20 + 0.0036 T[b]
NO_2 (g)	–33.2	–

[a] (c) = Crystalline, (g) = gas

[b] T = Absolute temperature

[c] Calculated from the discrete values

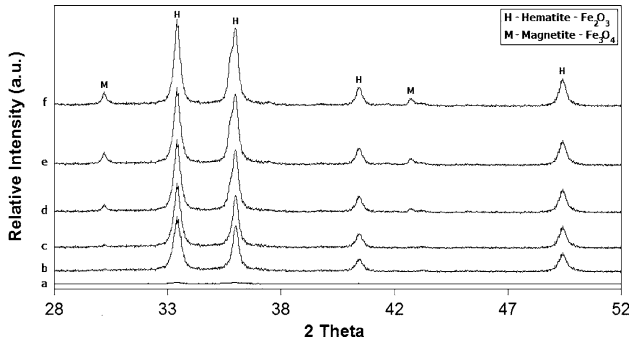

Fig. 4 Overlay of X-ray diffraction patterns of iron oxide ceramic powder as-synthesized: (a) fuel-lean reaction (L1: only hematite phase), (b) Stoichiometry reaction (S: hematite and magnetite), (c, d, e and f) fuel-rich (R1, R2, R3 and R4 respectively: hematite and magnetite phases)

This result suggests that the fuel-to-oxidizer interactions in the solution first lead to the formation of Fe_3O_4 that reacts further with the atmospheric O_2 to yield α-Fe_2O_3 phase compliant with Deshpande et al. [17].

As can be seen in the phase diagram of Fe and O, Fig. 5, the mixed-valence iron ion (II, III)-oxide corresponds to the coexistence of such phases in certain range of oxygen pressure and temperature.

Indeed, it is difficult to synthesize a single-phase crystalline Fe_3O_4 via solution combustion synthesis due to the fact that the nanoparticles tend to oxidize at the temperature and pressure of occurrence the combustion process.

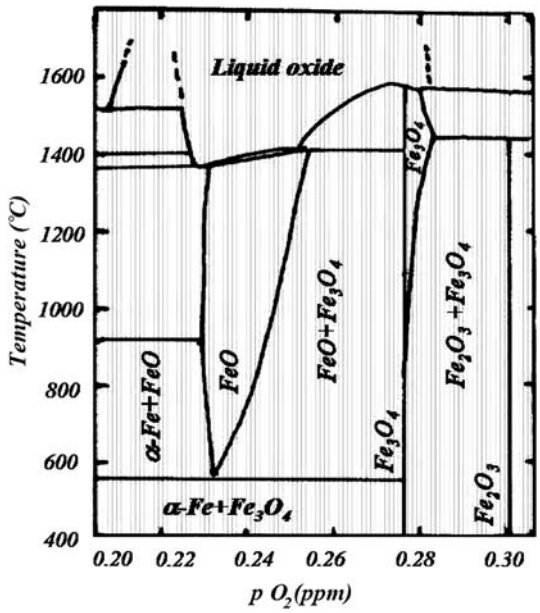

Fig. 5 Phase diagram of Fe and O [25]

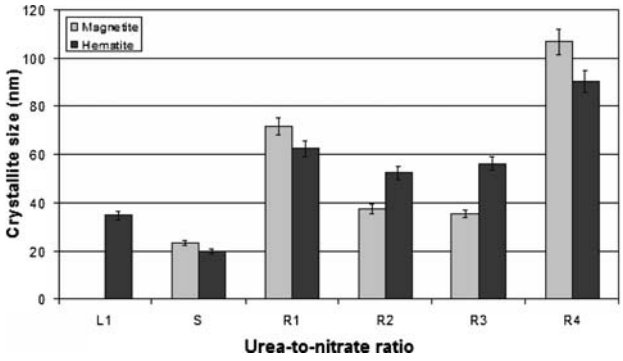

Fig. 6 Crystallite size for all urea-to-nitrate ratios

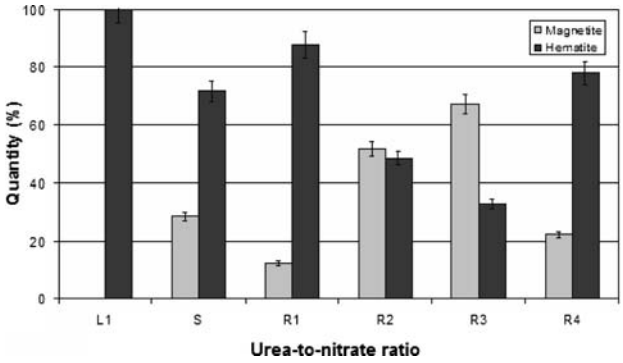

Fig. 7 Quantity corresponding each phase for all urea-to-nitrate ratios

The critical obstacle in converting α-Fe_2O_3 (hematite) to Fe_3O_4 (magnetite) is that formation of the latter phase is thermodynamically stable over a restricted pressure (≈0.277 ppm O_2) and low temperatures (<400 °C). In this work the atmosphere was not controlled for a given combustion temperature. The degree of conversion increases with the oxygen pressure as verified on zinc ferrite powders by Li et al. [26]. The oxygen pressure contributes substantially to the modifications that have been made in the combustion temperature and propagation of the combustion wave fronts.

Figure 6 lists the crystallite sizes of the as-synthesized powders prepared on different fuel-to-oxidant ratios. The stoichiometric reaction has the smallest crystallite size of bi-phase (Fe_3O_4 and α-Fe_2O_3) product.

Our results tend to indicate that the powders obtained through the fuel-rich ratios have the largest crystallite sizes as compared to those of stoichiometric and fuel-lean precursors. Relatively high combustion temperature obtainable by the fuel quantity can adversely affect powder characteristics such as an increase in the crystallite size. The creation of larger particles is attributed to the higher sintering temperatures.

The magnetite phase quantity is a determinant factor for magnetic behavior, as verified on Figs. 7 and 9, because R2 and R3 have a similar magnetic behavior and magnetite phase present, while L1, S, and R1 have the same performance of magnetization due to their magnetite presence. The crystallite size may influence saturation magnetization, which can be elucidated through the transition from mono- to multi-magnetic-domain behavior [27].

Possibly, there could be a competition between the effect of the magnetite phase formation and the crystallite size in influencing the magnetic performance of the powder product.

The SEM morphology of the agglomerates of the iron oxide is showed in Fig. 8. It revealed foamy agglomerated particles with a wide distribution and presence of some

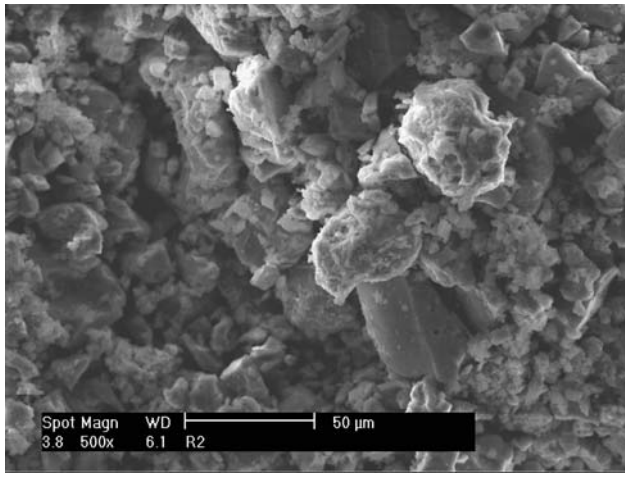

Fig. 8 SEM picture of iron oxide powder produced from stoichiometric reaction

voids in their structure. Formation of these features is attributed to the fact that the particles tend to aggregate and coarsen at the temperatures of the combustion synthesis process.

No significant differences came out of the fuel-to-oxidant ratios from all morphologies examined by the SEM.

Magnetic Properties

The magnetic properties of the synthesized iron oxide powders were investigated by VSM analyses. Figure 9 shows the hysteresis loops of the as-synthesized powders that exhibit quite low magnetization values. They do not achieve a saturation value even at 15,000 Oe. This is a typical characterization of soft magnetic materials. L1, S and R1 fuel-to-oxidant ratios have almost no remnant magnetization at zero magnetic field strength, which is an indication of superparamagnetism.

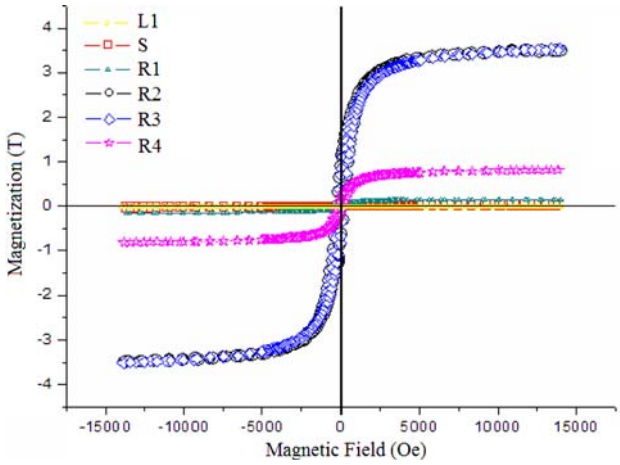

Fig. 9 Magnetization curves M as a function of applied field H

However, on powders synthesized under rich reactions (R2 and R3) with urea the saturation magnetization was notably elevated in comparison with other fuel-to-oxidant ratios studied. Practically they have some characteristics of hard magnetic materials. This result seems to be caused more by the dependence of the magnetite phase quantity than due to the presence of superparamagnetic particles.

The overall hysteresis loop of bi-phase mixture does not represent a simple sum of contributions corresponding to individual components, but is affected by interactions between magnetite and hematite crystallite sizes [28].

The impurity content or poor crystallization may also affect the magnetic behavior of the as-synthesized powders by reducing the maximum magnetization and increasing slightly the coercive force [16]. Here these contributions might be applied to magnetite and hematite powders.

In general, the maximum magnetization of the resulting powders showed a strong dependence on the fuel-to-oxidant ratio employed. The room temperature magnetization studies i.e. saturation magnetization, coercive force, and remanence ratio for the samples are summarized in Table 2.

Table 2 Magnetic hysteresis of samples

Urea-to-nitrate ratio	Saturation magnetization (M_s, T × 10^{-6})	Remnant magnetization (M_r, T × 10^{-6})	Squareness ratio (M_r/M_s)
L1	42.54	0.88	0.021
S	5.31	0.62	0.117
R1	75.27	0.09	0.241
R2	310.71	66.50	0.214
R3	326.71	61.80	0.189
R4	149.36	36.06	0.001

Conclusions

Nanocrystalline iron oxide (containing hematite and magnetite phases) was synthesized by solution combustion process. This method has the advantage that it can produce ultra-fine iron oxide powders fairly quickly. The size of the product particle increases when the ferrous ion is present in excess.

Thermodynamic modeling of the combustion reaction shows that when fuel-to-oxidant ratio increases the amount of gas produced and the heat of reaction also increase.

Acknowledgements Thanks are due to Undergraduate student Luciana J. Stein for combustion synthesis measurements, Eng. Hugo J. de Andrade for providing support on Scanning Electron Microscopy and Angelo R. Morrone for the aid in Vibrating Sample Magnetometer technique.

References

1. Li P, Miser DE, Rabiei S, Yadav RT, Hajaligol MR (2003) Appl Catal B: Environ 43(2):151
2. Potter MJ (2001) Iron oxide pigments. U.S. Geological Survey Minerals Yearbook, vol 1. 42 pp
3. Hsiang H, Yen F (2002) Ceram Int 29:1
4. Yang H, Guo Q, Teng X (2003) J Am Chem Soc 125:630
5. Saiyed ZM, Telang SD, Ramchand CN (2003) Biomagn Res Technol 18(1):1
6. Cheng F, Su C, Yang Y, Yeh C, Tsai C, Wu C, Wu M, Shieh D (2005) Biomaterials 7(26):729
7. Harris L (2002) Polymer stabilized magnetite nanoparticles and poly(propylene oxide) modified styrene-dimethacrylate networks. Doctoral Thesis, Virginia State University, Blacksburg, VI, USA, p 28
8. Meldrum FC, Kotov NA, Fendler JH (1994) Am Chem Soc 98:4506
9. Raming TP, Winnubst AJA, van Kats CM, Philipse AP (2002) J Colloid Interf Sci 249:346
10. Zhu Y, Wu Q (1999) J Nanopart Res 1:393
11. Patil KC, Aruna ST, Mimani T (2002) Curr Opin Solid State Mater Sci 6:507
12. Civera A, Pavese M, Saracco G, Specchia V (2003) Catal Today 83:199
13. Nagaveni K, Sivalingam G, Hegde MS, Madras G (2004) Appl Catal B: Environ 48:83
14. Xijuan Y, Pingbo X, Qingde S (2001) Phys Chem Chem Phys 3:5266
15. Suresh K, Patil K (1993) J Mater Sci Lett 12:572
16. Venkataraman A, Hiremath VA, Date SK, Kulkarni SD (2001) Bull Mater Sci 24:617
17. Deshpande K, Mukasyan A, Varma A (2004) Chem Mater 16:4896
18. Erri P, Pranda P, Varma A (2004) Ind Eng Chem Res43:3092
19. Bhaduri S, Bhaduri SB, Zhou E (1998) J Mater Res 13:156
20. Purohit RD, Sharma BP, Pillai KT, Tyagi AK (2001) Mater Res Bull 36:2711
21. Toniolo JC, Lima MD, Takimi AS, Bergmann CP (2005) Mater Res Bull 40:561
22. Souza VC, Segadães AM, Morelli MR, Kiminami RHGA (1999) Int J Inorg Mater 1:235

23. Perry RH, Chilton CH (1973) Chemical engineers handbook, 5th edn. McGraw-Hill, New York, p 197
24. Dean JA (ed) (1979) Lange's handbook of chemistry, 12th edn. McGraw-Hill, New York
25. Sundman B (1991) J Phase Equilib 127
26. Li Y, Zhao J, Jiang J, He X (2003) Mater Chem Phys 82:991
27. Albuquerque AS, Ardisson JD, Macedo WAA (2000) J Appl Phys 87:4352
28. Hejda P, Kapička A, Petrovský E, Sjöberg B (1994) IEEE Trans 2(30):881